SLAC-PUB-15841

Speed Limit of the Insulator to Metal Transition in Magnetite

S. de Jong *[1], R. Kukreja *[1,2], C. Trabant[3,4,5], N. Pontius[4], C. F. Chang[3,6], T. Kachel[4], M. Beye[4], F. Sorgenfrei[4,7] , C. H. Back[1,8], B. Bräuer[1], W. F. Schlotter[9], J. J. Turner[9], O. Krupin[9,10], M. Doehler[3], D. Zhu[1], M. A. Hossain[1], A. O. Scherz[1,10], D. Fausti[11,12], F. Novelli[12], M. Esposito[11,12], W. S. Lee[1], Y. D. Chuang[13] , D. H. Lu[14], R. G. Moore[1], M. Yi[1], M. Trigo[1], P. Kirchmann[1], L. Pathey[15], M. S. Golden[1,16], M. Buchholz[3], P. Metcalf[17], F. Parmigiani[11,12], W. Wurth[7], A. Föhlisch[4,5], C. Schüßler-Langeheine[3, 4, ‡] and H. A. Dürr[1, †]

[1] *Stanford Institute for Energy and Materials Sciences, SLAC National Accelerator Laboratory, 2575 Sand Hill Road, Menlo Park, CA 94025, USA*
[2] *Stanford University, Department of Materials Science and Engineering, CA 94305, USA*
[3] *Universität zu Köln, II. Physikalisches Institut, Zülpicher Straße 77, 50937 Köln, Germany*
[4] *Helmholtz-Zentrum Berlin für Materialien und Energie, Albert-Einstein-Str. 15, 12489 Berlin*
[5] *Universität Potsdam, Institut für Physik und Astronomie, Karl-Liebknecht-Strasse 24-25, 14476 Potsdam, Germany*
[6] Max Planck Institut für Chemische Physik fester Stoffe (MPI CPfS), Nöthnitzer Str. 40, 01187 Dresden, Germany
[7] *Universität Hamburg, Department of Physics and Center for Free-Electron Laser Science, Luruper Chaussee 149, 22761 Hamburg, Germany*
[8] *Universität Regensburg, Physikalisches Institut, Universitätsstrasse 31, 93053 Regensburg, Germany*
[9] *Linac Coherent Light Source, SLAC National Accelerator Laboratory, 2575 Sand Hill Road, Menlo Park, CA 94025, USA*
[10] *European XFEL GmbH, Albert-Einstein-Ring 19, 22761 Hamburg, Germany*
[11] *Department of Physics, University of Trieste, Trieste, Italy*
[12] *Elettra-Sincrotrone Trieste SCnA, Basovizza I-34012, Italy*
[13] *Advanced Light Source, LBNL, 1 Cyclotron Rd, Berkeley, CA 94720 USA*
[14] *Stanford Synchrotron Radiation Lightsource, SLAC National Accelerator Laboratory, 2575 Sand Hill Road, Menlo Park, CA 94025, USA*
[15] *SwissFEL, Paul Scherrer Institut, 5232 Villigen PSI, Switzerland*
[16] *University of Amsterdam, Van der Waals-Zeeman Institute, Science Park 904, 1098 XH Amsterdam, The Netherlands*
[17] *Purdue University, School of Materials Engineering, West Lafayette, Indiana 47907, USA*
* *These authors contributed equally to this work*
‡ *Email: christian.schuessler@helmholtz-berlin.de*
† *Email: hdurr@slac.stanford.edu*

Submitted to Nature Materials.

Work supported in part by US Department of Energy under contract DE-AC02-76SF00515.

As the oldest known magnetic material, magnetite (Fe_3O_4) has fascinated mankind for millennia. As the first oxide in which a relationship between electrical conductivity and fluctuating/localized electronic order was shown [1], magnetite represents a model system for understanding correlated oxides in general. Nevertheless, the exact mechanism of the insulator-metal, or Verwey, transition has long remained inaccessible [2-8]. Recently, three-Fe-site lattice distortions called trimerons were identified as the characteristic building blocks of the low-temperature insulating electronically ordered phase [9]. Here we investigate the Verwey transition with pump-probe x-ray diffraction and optical reflectivity techniques, and show how trimerons become mobile across the insulator-metal transition. We find this to be a two-step process. After an initial 300 femtosecond destruction of individual trimerons, phase separation occurs on a 1.5 ± 0.2 picosecond timescale to yield residual insulating and metallic regions. This work establishes the speed limit for switching in future oxide electronics [10]

Crossing the Verwey transition of magnetite (T_V = 123 K) from above, charge fluctuations marking the conducting state freeze into an electronically ordered structure with octahedrally coordinated Fe^{2+} and Fe^{3+} sites, resulting in a hundred-fold increase in the resistivity [1]. This transition is accompanied by a change in the crystal symmetry from a high-temperature cubic inverse spinel to a monoclinic phase, the fine details of which have eluded crystallographers for decades. An important step was taken recently, demonstrating that the low-temperature structure consists of a network of three-Fe-site distortions dubbed trimerons, encompassing two outer 3+ and a central 2+ octahedral Fe_B site ions [9]. In addition, the t_{2g} orbitals within a trimeron are ordered, meaning that the trimeron lattice (see Fig. 1) is the true microscopic face of the electronic order in magnetite. Fluctuations to this trimeron order have been observed up to 80 K above T_V in neutron scattering studies [11, 12].

In many oxide materials [13, 14] the insulator-metal transition has been discussed in terms of freezing in fluctuating lattice and electronic (charge, spin and orbital) order, sometimes in combination with the occurrence of phase separation [15, 16]. However, due to the many competing degrees of freedom, the close energetic proximity of the different phases often obscures the exact nature of these phase transitions as they are probed in thermal equilibrium [17]. In magnetite, the Verwey transition does not involve changes in the spin ordering, allowing a focus purely on the role of the lattice and electronic ordering. As such magnetite serves as a model system to understand the mechanism behind the insulator-metal transition for a large group of materials.

Here we show how the insulator-metal transition in magnetite can be unraveled in the time domain. We utilize time-resolved x-ray diffraction [18] and optical reflectivity [19,20] to disentangle the lattice and electronic degrees of freedom and study the role of phase separation in the Verwey transition. Starting from the insulating phase at 80 K, energy is rapidly injected into the electronic system via femtosecond (fs) laser excitation. The lattice and electronic order responses are probed via soft x-ray diffraction at the Linac Coherent Light Source (LCLS) [21] (see methods and Fig. 1). We show that the insulator-metal transition proceeds in two distinctly different stages. An ultrafast (< 300 fs) punching of holes into the quasi-static trimeron lattice is the first step, followed by a 1.5 ± 0.2 picosecond (ps) rearrangement of residual trimerons. In the following, we will characterize these two steps by first monitoring the lattice and electronic order parameters (diffraction intensity) succeeded by discussion of the electronic order coherence length. The latter, together with time-resolved optical reflectivity, reveal a ps phase segregation into insulating domains of residual electronic order and a percolative network of coexisting metallic domains supporting polaronic charge transport.

The low-temperature monoclinic structure is established through freezing-in of various phonon modes across T_V [9]. Some of these frozen phonons (most notably the X_1 and Δ_5 modes [22]) act as primary order parameters for the insulating trimeron phase. This gives rise to low-temperature Bragg peaks that are forbidden in the cubic high-temperature phase (see supplementary information). Here we monitor the low-temperature lattice order via (001) and (110) Bragg diffraction and the electronic order via the $(00^1/_2)$ Bragg peak, visible when the x-ray energy is tuned to the electronic 2p-3d core-valence resonance of the B-site Fe atoms (see methods and supplementary information).

Fig. 2a shows the temporal evolution of the lattice order by means of the scattering intensity for the (001) Bragg peak for three different pump fluences. The pump pulse triggers electronic excitations within the trimeron lattice, resulting in the creation of 'trimeron holes' in the network. This expresses itself as the ultrafast drop in scattering intensity (denoted A, orange arrow). This ultrafast response of a sub-set of atomic displacements attests to the strong coupling between electronic and lattice degrees of freedom in the system. After the initial, ultrafast intensity drop seen for all fluences, a further ps evolution takes place. Its nature depends on the pump fluence. At low fluence, a thermally equilibrated trimeron lattice reasserts itself after about 1 ps, leading to an increase in scattering intensity (top curve in Fig. 2a). We note that the initial low-temperature state is re-established only after microseconds due to the low thermal conductivity [18] of the system. For higher fluence (lowest curve in Fig. 2a), the ps behavior is different. It displays a monotonously continuing reduction in diffraction intensity with increasing pump-probe delay time (parameter B, purple shading). Fig. 2b shows the resulting decomposition of the time profiles into the two parameters, A and B, as a function of pump fluence. The figure also demonstrates that the behavior of the (110) lattice Bragg peak is identical to that of the (001). As the next step, we add the analysis of time-traces from the $(00^1/_2)$ electronic order diffraction intensity [23-25] into Fig. 2b. It is immediately evident that all the data can be collapsed onto a single, universal plot. The continued ps decay B displays a clear threshold pump fluence of 1.3 ±

0.1 mJ cm^{-2}. The threshold value is a surprisingly good match to the energy required to drive magnetite from 80 K across the Verwey transition in thermodynamic equilibrium (see supplementary information).

Up to this point, we have shown that optical excitation launches a strongly coupled charge-lattice motion, locally destroying the trimeron order. Now we address the question whether this process can instigate metallic behavior. By probing the coherence length of the electronically ordered phase after the optical excitation, we show that the system segregates into coexisting metallic and insulating domains on a 1.5 ± 0.2 ps timescale. In Fig. 3 we show the evolution of the coherence length, λ_{coh}, extracted from the diffraction peak width and the change in the monoclinic tilt angle, $\Delta\beta$. Fig. 1 shows that a $\Delta\beta$ change results in a characteristic shift of the diffraction peak (see supplementary information). The relative diffraction intensity (dashed brown line in Fig. 3) is strongly suppressed within 300 fs of the optical excitation pulse. The intensity goes on to reach values below 5% of the static value on the ps timescale. In contrast to the fast intensity quench, the changes of $\Delta\beta$ and λ_{coh} display a very different characteristic timescale of 1.5 ± 0.2 ps for this pump fluence. Moreover, $\Delta\beta$ and λ_{coh} changes are only observed later than 200 fs (the earliest data point following optical excitation included in Fig. 3). This means that on the timescale of the ultrafast intensity quench, the low-temperature monoclinic lattice tilt angle and the trimeron lattice coherence length remain unchanged with respect to the static case. We note that the observed static coherence length of λ_{coh} = 385 ± 10 nm is in good agreement with literature values [3].

The observed shrinking correlation length of the insulating trimeron lattice indicates island formation, providing space for a coexisting, metallic phase. We used optical reflectivity to detect its existence. In thermal equilibrium, the transition from insulating to metallic behaviour is accompanied by the appearance of a spectral feature centered at 725 nm [19]. We found the same feature to appear in time-resolved, pump-probe experiments with a 1.5 ± 0.2 ps time constant

(see supplementary information). The observed delayed onset and subsequent increase of metallic character (red line in Fig. 3) mirrors the decay of the insulating phase. The fluence dependence (right inset in Fig. 3) shows that the metallic phase is fully developed above 4 mJ cm^{-2}.

Therefore, on short timescales shooting holes into the trimeron lattice weakens the network, but does not destroy its long-range order. This behaviour of negligible change in correlation length despite strong reduction in intensity has also been observed in nickelates [26], where it is associated with small fluctuations in amplitude and phase of charge order. In contrast, in magnetite, large phase fluctuations in the electronic order result in the observed ps decrease of the correlation length in Fig. 3. Thus a `transformational regime' is entered on the ps timescale that is marked by a break-up of the trimeron lattice into patches separated by a coexisting metallic phase which scrambles the phase coherence of the surviving trimerons islands (see Fig. 4). This is accompanied by a relaxation of the monoclinic lattice tilt $\Delta\beta$ in the trimeron islands towards the right-angle cubic value (see schematics in Fig. 1). After 5 ps in Fig 3, the deviation from the cubic lattice angle is 0.11° compared to 0.23° for the static low-temperature case. One of the most remarkable aspects of the data of Fig. 3 is that the lattice transformation towards the cubic ideal does not happen synchronously with the ultrafast trimeron annihilation process. The transformational, ps regime is only entered at pump fluences above the threshold value, since both λ_{coh} and the monoclinic tilt change only above 1.3 ± 0.1 mJ cm^{-2} (left inset to Fig. 3), in agreement with the minimal fluence for metallic character seen in the optical reflectivity (right inset to Fig. 3).

Bringing together all pieces of the puzzle, as shown in Fig. 4, we can now describe, step-by-step, the energy-flow processes following fs optical excitation of the electronically ordered Fe B-sites in magnetite:

(1) On a fs timescale, the optical pump pulse induces transitions in the electronic system (red arrows in panel A of Fig. 4), leading to the creation of holes in the trimeron lattice.

(2) This process, which represents trimeron annihilation (overlap area in panel A of Fig. 4), triggers relaxation of the monoclinic distortions related to a subset of the frozen phonon modes, namely the ones with the largest amplitude situated on the end points of the trimerons [9] (see supplementary information). It is the frozen X_1 and Δ_5 modes that dominate the monitored diffraction peaks (see supplementary information). The energy of these X_1 and Δ_5 modes is between 10 to 30 meV [27], yielding characteristic vibrational timescales between 400 and 150 fs. We note that possible coherent oscillations of these modes would be smeared out due to the time resolution (~300 fs) of our experiment.

(3) After 300 fs, the residual trimeron lattice retains the long-range order of the insulating phase (panel [B] of Fig. 4), albeit possessing excess energy that is dissipated on a longer (ps) timescale.

(4) If the pump fluence is low, the trimeron lattice then recovers and the system simply returns to a warmer version of the electronically ordered insulating state, via equilibration of the hot phonon modes. Yet the long range coherence of all the other frozen displacement modes of the monoclinic structure is still preserved.

(5) For a pump fluence above threshold, the excess energy is sufficient to drive the system through a point of no return. We note that the dynamics of this unfreezing depends on the starting temperature before the pump: lower temperatures requiring larger pump fluences (see Fig. S2 in the supplementary information) Thus, for 80K starting temperature, the transformational regime (panel [C] of Fig. 4) is entered on a characteristic timescale of 1.5 ± 0.2 ps. The observed relaxation of the monoclinic tilt indicates the melting of the Γ-mode distortions (see supplementary information) on this time scale. The 80 K threshold fluence of 1.3 ± 0.1 mJ cm^{-2} corresponds to the absorption of about one photon per monoclinic unit cell, containing 30

trimeron sites (see supplementary information). A single 1.5 eV photon can create about 5-10 electron-hole pairs above the band gap [5, 19], thus the threshold fluence corresponds to the destruction of about 1 in 4 trimerons.

(6) This transformational process switches the system from being a long-range ordered trimeron lattice (blue in Fig. 4) with holes in it (dashed), into a patchwork of modified but still electronically ordered remnants (purple in panel [C] of Fig. 4), with structural parameters leaning towards those of the charge fluctuating, conducting cubic matrix in which they reside (red, seen in reflectivity). This transition from the residual coherent trimeron network to a phase segregated state has to proceed via coalescence of `trimeron-holes' and thus involves the hopping of charges together with their associated lattice distortions between trimeron lattice sites. We note that the electronic order observed after 1.5 ps could - in principle - be a different one to that in the ground-state. However, the optical data as well as the observed reduction of the monoclinic tilt angle indicates that the 800 nm pump drives the system (partially) into the high-temperature phase. The fact that electronic order is still observed at such ps timescales clearly indicates the existence of insulating regions in the sample. Hence, the observed B process is the signature of polaronic transport, further eroding the ordered regions on a ps timescale after the optical excitation. This polaronic hopping timescale matches well with the charge density relaxation time seen in inelastic neutron scattering associated with fluctuating trimeron order above T_V [12]. These observations all point to the fact that the threshold fluence, translating to trimeron lattice collapse for a volume fraction below ~ 75%, is required to create a percolative network of charge-fluctuating, metallic, sites in the trimeron matrix (see supplementary information).

This pump-induced transformation can thus be regarded as a non-equilibrium version of the thermodynamic Verwey transition seen in the conductivity-temperature phase diagram of magnetite. Consequently, the data show how magnetite dynamically evolves towards its energy minimum during the Verwey transition: initially holes in the long-range ordered trimeron lattice

allow the trimerons to become mobile and form shorter-range ordered domains surrounded by charge fluctuating regions. The coalescence of the remaining trimerons, driven by their desire to keep the monoclinic distortion intact, is connected to the organization of hundreds of atoms involved in the frozen displacement modes of the monoclinic structure. The bulk metallic phase is reached as soon as the charge-fluctuating regions form a percolation pathway through the magnetite crystal.

In conclusion, our experiments show that insulating, electronically ordered, low-temperature magnetite displays phase segregation on a 1.5 ± 0.2 ps timescale following ultrafast (< 300 fs) laser induced trimeron hole creation. We identify a residual low-temperature, insulating phase embedded in a phase resembling the high-temperature metallic lattice, the latter forming a percolative charge-fluctuating path throughout the sample. The switching of conductivity in such an archetypal complex oxide at the picosecond timescale clocks these systems faster than the best graphene transistors [28] developed to date. The understanding we have gained here as regards to how the transformation between the two states straddling the Verwey transition actually takes place could aid in the choice and design of oxide materials aiming at harnessing the enormous differences in electrical conductivity available in these systems.

METHODS

Time-resolved resonant soft x-ray diffraction measurements were carried out at the SXR beamline [29] of the Linac Coherent Light Source (LCLS), using monochromatised x-rays of 10 fs pulse duration with a repetition rate of 60 Hz and a bandwidth of 400 meV at the Fe L_3 edge (707 eV photon energy). A pump-laser with photon energy $h\nu$ = 1.55 eV and 70 fs pulse duration was synchronized to the x-ray pulses. The scattering data were intensity normalized on a shot-by-shot basis and corrected for jitter in the arrival time of the electron bunch of the free electron

laser. The shortest measured timescale of < 300 fs represents an upper limit of the remaining x-ray to optical pulse arrival time jitter.

The x-ray and pump laser foci on the sample had diameters of 200 and 500 μm, respectively. Pump fluence values given here are depth-corrected, taking the penetration depth of the x-ray probe into account (see supplementary information), thus making diffraction data measured at different x-ray energies directly comparable. Diffraction data were acquired using the RSXS endstation [30], equipped with a fast avalanche photodiode (integrating over the entire diffraction peak) and a two dimensional fast CCD camera both shielded from the optical pump laser by an Al window. Fig. 1 shows a sketch of the experimental setup. Synthetic magnetite single crystals were cleaved in air before introducing them within minutes into an ultra-high vacuum environment with a base pressure of 1×10^{-9} mbar. All displayed data were collected at a base temperature of 80 K. During the x-ray diffraction measurements, we did not find any evidence for the appearance of structurally twinned domains within the spatial extent of the x-ray photon spot (see supplementary information).

The primary order parameters of the magnetite cubic-to-monoclinic lattice distortion are the cubic X and Δ phonon modes. These modes are strongly coupled with (001) and (110) lattice reflections (see Fig. S4 in the supplementary information). Note: cubic notation is used throughout the paper. The monoclinic lattice order of magnetite was non-resonantly probed at the (001) and (110) reflections with 800 eV and 1200 eV x-rays, respectively. Electronic order below T_V is characterized by the appearance of a $(00^1/_2)$ ordering period and was selectively probed on resonance at the Fe L_3-edge ($h\nu$ = 707 and 708 eV) [24, 25]. The CCD detector was used to record the data for the $(00^1/_2)$ reflection at the Fe L_3-edge presented in Figs. 1 and 3. All other data presented were recorded using the photodiode detector.

Time-resolved optical reflectivity was measured as described in Ref. [20] (see supplementary information) using an amplified Ti:sapphire laser system with ~80 fs pulse duration operating at 250 kHz. 800 nm pump and 500-800 nm probe beams were focused to spot diameters of ~110 and 90 μm, respectively. The sample was identical to the single crystal used for the experiments at the LCLS. The optical signature of conductivity was probed in a 700 to 750 nm wavelength interval following Ref. [19].

REFERENCES

[1] Verwey, E. J. W. Electronic conduction of magnetite (Fe_3O_4) and its transition point at low temperatures. *Nature* **144,** 328 (1939).

[2] Nazarenko, E. *et al.* Resonant X-Ray Diffraction Studies on the Charge Ordering in Magnetite. *Phys. Rev. Lett.* **97,** 056403 (2006).

[3] Lorenzo, J. E. *et al.* Charge and Orbital Correlations at and above the Verwey Phase Transition in Magnetite. *Phys. Rev. Lett.* **101,** 226401 (2008).

[4] Garcia, J. *et al.* Reexamination of the Temperature Dependences of Resonant Reflections in Highly Stoichiometric Magnetite. *Phys. Rev. Lett.* **102,** 176405 (2009).

[5] Piekarz, P., Parlinski, K. & Oles, A. M. Origin of the Verwey transition in magnetite: Group theory, electronic structure, and lattice dynamics study. *Phys. Rev. B* **76,** 165124 (2007).

[6] Uzu, H. & Tanaka, A. Complex-orbital order in Fe_3O_4 and mechanism of the Verwey transition. *J. Phys. Soc. of Japan* **77,** 074711 (2008).

[7] Garcia, J. & Subias, G. The Verwey transition - a new perspective. *Journal of Physics: Condensed Matter* **16,** R145 (2004).

[8] Weng, S.-C., *et al.* Direct Observation of Charge Ordering in Magnetite Using Resonant Multiwave X-Ray Diffraction. *Phys. Rev. Lett.* **108,** 146404 (2012).

[9] Senn, M. S., Wright, J. P. & Attfield, J. P. Charge order and three-site distortions in the Verwey structure of magnetite. *Nature* **481,** 173 (2012).

[10] Yang, Z., Ko, C. & Ramanatha, S. Oxide Electronics Utilizing Ultrafast Metal-Insulator Transitions. *Annual Review of Materials Research* **41,** 337 (2011).

[11] Fujii, Y., Shirane, G. & Yamada, Y. Study of the 123-K phase transition of magnetite by critical neutron scattering. *Phys. Rev. B* **11,** 2036 (1975).

[12] Shapiro, S. M., Iizumi, M. & Shirane, G. Neutron scattering study of the diffuse critical scattering associated with the Verwey transition in magnetite. *Phys. Rev. B* **14,** 200 (1976).

[13] Weber, F. *et al.* Signature of checkerboard fluctuations in the phonon spectra of a possible polaronic metal $La_{1.2}Sr_{1.8}Mn_2O_7$. *Nature Mater.* **8,** 798 (2009).

[14] Imada, M., Fujimori, A. & Tokura, Y. Metal insulator transitions. *Rev. Mod. Phys.* **70,** 1039 (1998).

[15] Uehara, M., Mori, S., Chen, C. H. & Cheong, S.-W. Percolative phase separation underlies colossal magnetoresistance in mixed valent mangatite. *Nature* **399,** 560 (1999).

[16] Lai, K., *et al.* Mesoscopic Percolating Resistance Network in a Strained Manganite Thin Film. *Science* **329,** 190 (2010).

[17] Massee, F. *et al.* Bilayer manganites: polarons on the verge of a metallic breakdown. *Nature Phys.* **7,** 560 (2011).

[18] Pontius, N. *et al.* Time-resolved resonant soft x-ray diffraction with free-electron lasers: Femtosecond dynamics across the Verwey transition in magnetite. *Appl. Phys. Lett.* **98,** 182504 (2011).

[19] Park, S. K., Ishikawa, T. & Tokura, Y. Charge-gap formation upon the Verwey transition in Fe_3O_4. *Phys. Rev. B* **58,** 3717 (1998).

[20] Novelli F., *et al.* Ultrafast optical spectroscopy of the lowest energy excitations in the Mott insulator compound YVO_3: Evidence for Hubbard-type excitons, *Phys. Rev. B* **86**, 165135 (2012).

[21] Emma, P. *et al.* First lasing and operation of an Angstrom-wavelength free-electron laser. *Nature Photon*. **4,** 641 (2010).

[22] Blasco, J., Garcia, J. & Subias, G. Structural transformation in magnetite below the Verwey transition. *Phys. Rev. B* **83,** 104105 (2011).

[23] Huang, D. J. *et al.* Charge-Orbital Ordering and Verwey Transition in Magnetite Measured by Resonant Soft X-Ray Scattering. *Phys. Rev. Lett.* **96,** 096401 (2006).

[24] Schlappa, J. *et al.* Direct Observation of t_{2g} Orbital Ordering in Magnetite. *Phys. Rev. Lett*. **100,** 026406 (2008).

[25] Tanaka, A. *et al.* Symmetry of Orbital Order in Fe_3O_4 Studied by Fe $L_{2,3}$ Resonant X-Ray Diffraction. *Phys. Rev. Lett.* **108,** 227203 (2012).

[26] Lee, W. S. *et al.* Phase fluctuations and the absence of topological defects in a photo-excited charge-ordered nickelate. *Nature Commun.* **3,** 838 (2012).

[27] Samuelson, E. J. & Steinsvoll O. Low-Energy Phonons in Magnetite. *Phys. Stat. Sol. (b)* **61,** 615 (1974).

[28] Wu, Y. *et al.* High frequency scaled graphene transistors on diamond-like carbon. *Nature (London)* **472,** 74 (2011).

[29] Heimann, P. *et al.* Linac Coherent Light Source soft x-ray materials science instrument optical design and monochromator commissioning. *Rev. Sci. Instrum*. **82,** 093104 (2011).

[30] Doering, D. *et al.* Development of a compact fast CCD camera and resonant soft x-ray scattering endstation for time-resolved pump-probe experiments, *Rev. Sci. Instrum.* **82**, 073303 (2011).

ACKNOWLEDGMENTS

Research at Stanford was supported through the Stanford Institute for Materials and Energy Sciences (SIMES) under contract DE-AC02-76SF00515 and the Linac Coherent Light Source (LCLS) by the US Department of Energy, Office of Basic Energy Sciences. Portions of this research were carried out on the SXR Instrument at the LCLS, a division of SLAC National Accelerator Laboratory and an Office of Science user facility operated by Stanford University for the U.S. Department of Energy. The SXR Instrument is funded by a consortium whose membership includes the LCLS, Stanford University through the Stanford Institute for Materials Energy Sciences (SIMES), Lawrence Berkeley National Laboratory (LBNL, contract number DE-AC02-05CH11231), University of Hamburg through the BMBF priority program FSP 301, and the Center for Free Electron Laser Science (CFEL). MSG's stay at SLAC was made possible by support from FOM/NWO and the Helmholtz Virtual Institute Dynamic Pathways in Multidimensional Landscapes. The Cologne team was supported by the DFG through SFB 608 and by the BMBF (contract 05K10PK2). The research leading to the time-resolved optical experiment, performed by the Elettra-Sincrotrone Trieste and University of Trieste team, was supported by European Union Seventh Framework Programme [FP7/2007-2013] under grant

agreement number 280555 and by the Italian Ministry of University and Research under grant numbers: FIRB-RBAP045JF2 and FIRB-RBAP06AWK3. DF, FN, ME, and FP thank Federico Cilento and Francesco Randi for technical support.

AUTHOR CONTRIBUTIONS

HAD, AF, CS-L and WW conceived and planned the experiments. All authors except MSG carried out the experiment. WFS, JJT, OK, MT and PK provided excellent experimental guidance for using the SXR beamline and the LCLS optical laser system. WSL, YDC, DHL, RGM, MY and LP provided excellent support for the RSXS end station. SdJ and RK performed the data analysis. DF, FN, ME, and FP performed the time-resolved optical experiments and interpreted the optical data. SdJ, RK, MSG, CS-L and HAD wrote the manuscript with help and input from all authors.

COMPETING FINANCIAL INTERESTS

The authors declare to have no competing interests as defined by Nature Publishing Group, or any other interests that might be perceived to influence the results and/or discussion reported in this article.

ADDITIONAL INFORMATION

Additional information Supplementary information is available in the online version of the paper. Reprints and permissions information is available online at www.nature.com/reprints. Correspondence and requests for materials should be addressed to H.A.D, email:

hdurr@slac.stanford.edu, or C.S.-L., email: christian.schuessler@helmholtz-berlin.de

Figure legends

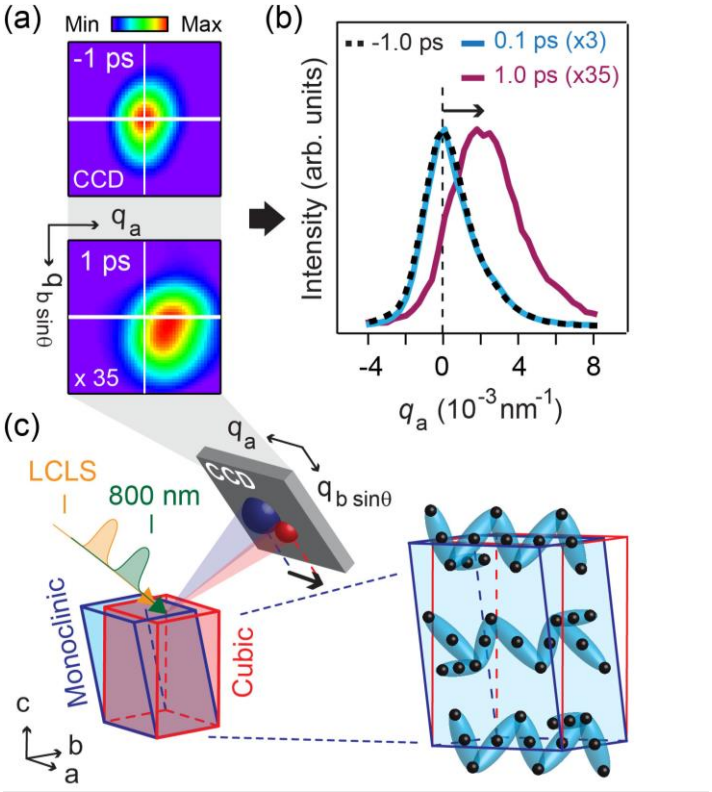

FIG. 1: Experimental optical pump – x-ray probe setup and response of the soft x-ray diffraction intensity from the monoclinic reflections of the low temperature phase of Fe_3O_4 upon optical pumping. (a) CCD detector images of the $(00^1/_2)$ electronic order recorded at the Fe L_3-edge before and after pumping with 4.9 mJ cm^{-2}. The pump-induced shift of the diffraction peak shows a clear in-plane component along q_a while the orthogonal direction is a superposition of in-plane (q_a) and out-of-plane (q_c) directions. (b) Horizontal line-scans of the $(00^1/_2)$ peak at q_b = 0 before 0 fs, at 0.1 ps and at 1 ps pump-probe delay time. (c) Sketch of the experimental setup. The magnetite crystal is shown as the blue (red) block in the monoclinic (cubic) structure. Inset: Low temperature unit cell with the electronically ordered trimeron lattice represented using blue ellipsoids after Ref. [9].

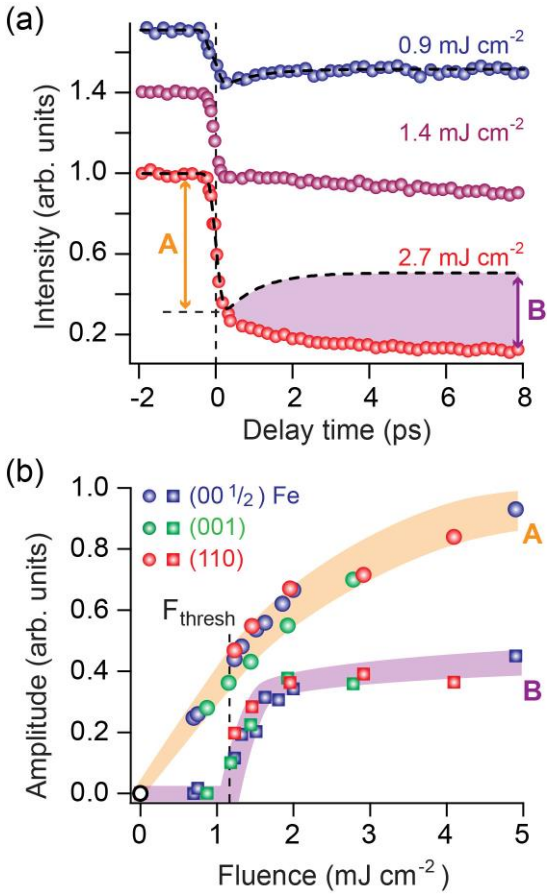

FIG. 2: Differing femtosecond and picosecond responses for the decay of the trimeron-related x-ray diffraction intensity. (a) Normalized (001) diffraction intensity versus time delay for pump fluence values as indicated (traces offset). The dashed line fits extract the characteristic timescales for pump fluences below 1.3 ± 0.1 mJ cm^{-2}. The orange arrow indicates a strong quench (A) of the diffraction from the ordered trimeron lattice in the first 300 fs. For longer times and pump fluences above 1.3 ± 0.1 mJ cm^{-2} the signal from the remnant trimeron lattice decays monotonically (B process defined as the difference between high- and extrapolated low-fluence behaviours, purple shading). (b) Pump fluence dependence of the fast (t < 300 fs) intensity drop A (orange arrow) and the slower intensity decay B (purple shading) of the diffraction intensity from the magnetite trimeron lattice from time traces like those shown in (a). The fast quench (A) is present for all fluences. The slower B decay appears only above a threshold pump fluence F_{thresh} = 1.3 ± 0.1 mJ cm^{-2}. This threshold shifts to higher pump fluences with decreasing initial sample temperatures (see supplementary information).

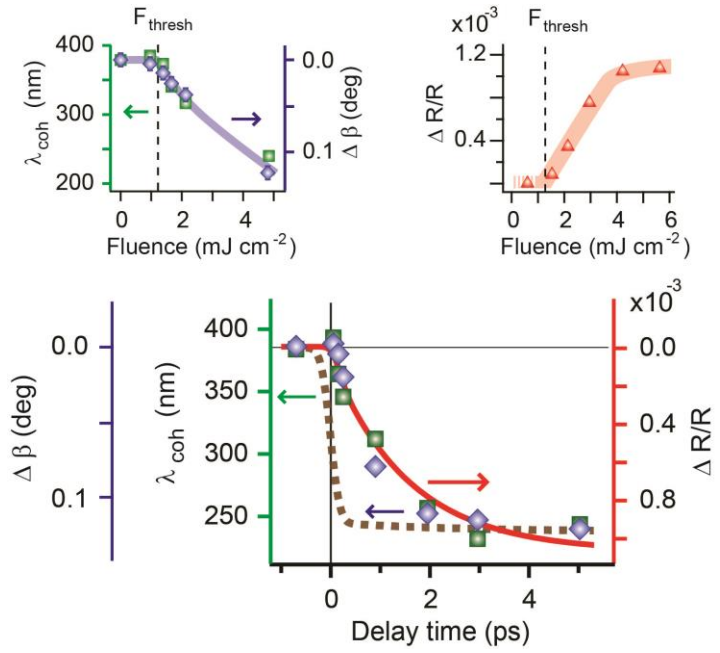

FIG. 3: Fast trimeron lattice quench followed by a ps transformational process. The figure compares x-ray data (blue/green symbols and brown line) taken at the $(00^1/_2)$ reflection (Fe L_3-edge) and optical reflectivity (red line, representing an exponential fit to the data in the supplementary information). The trimeron-order coherence length is derived as $\lambda_{coh} = 2\pi/\text{FWHM}$ with FWHM being the full width at half maximum of the diffraction data shown in Fig. 1b. Statistical errors in determining λ_{coh} and the change in monoclinic tilt angle, $\Delta\beta$, are given by the respective symbol sizes. The reductions in λ_{coh} and $\Delta\beta$ occur concomitant with the increase of $\Delta R/R$ with a time constant of 1.5 ± 0.2 ps. as shown by the red line (see supplementary information Fig. S3). This decay occurs with a delayed onset as clearly indicated by the unchanged λ_{coh} and $\Delta\beta$ values at 200 fs time delay (see Fig. 1b) and reflects the structural modifications towards the cubic lattice where metallic charge fluctuations reduce the coherence of the remnant patches of electronic order. As a comparison: the trimeron lattice diffraction intensity versus time (dashed brown solid line in arbitrary units centered at 0 fs time delay) shows a fast quench reflecting the time resolution of the experiment. The x-ray data were taken with a pump fuence of 4.9 mJ cm^{-2}. Left inset: Fluence dependent λ_{coh} and $\Delta\beta$ data taken at a

fixed delay time of 5 ps. The data show a threshold fluence, $F_{thres} = 1.3 \pm 0.1$ mJ cm^{-2}, above which the diffraction peaks display a change of the monoclinic angle $\Delta\beta$ (0.23° would correspond to the cubic case). The diffraction peaks also broaden linked to a reduction of the coherence length of the trimeron lattice remnants, λ_{coh}, by up to 40%. Right inset: Fluence dependent $\Delta R/R$ data taken at a fixed delay time of 5 ps, probing the onset of the metallic phase above 1.3 ± 0.1 mJ cm^{-2} (see supplementary information).

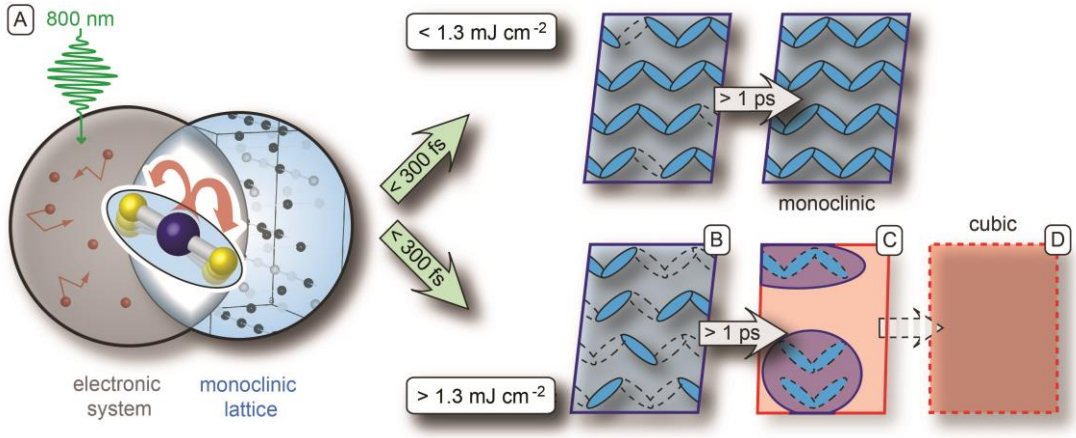

FIG. 4: Summary of the workings of the Verwey transition in non-equilibrium pump-probe form. (A) ultrafast trimeron annihilation due to laser excited Fe^{2+}-Fe^{3+} charge transfer launches strongly coupled electronic and lattice dynamics. For a pump fluence above 1.3 ± 0.1 mJ cm^{-2} trimeron holes (B) transform with a time constant of 1.5 ± 0.2 ps to a state with shrinking patches of remnant phase-scrambled electronic order as shown in (C). Its structure is approaching that of the cubic case, embedded in a network supporting mobile charge fluctuations (red) derived from the melting of the trimeron vacancies in (B). The end of the line would be the fully metallic, cubic phase (D).